Integrated Modeling for Prediction of Optimized ITER Performance

A.H. KRITZ[1], T. RAFIQ[1], C.E. KESSEL[2], G. BATEMAN[1], D.C. McCUNE[2], R.V.BUDNY[2], A.Y. PANKIN[1], D. CAMPBELL[3], T. CASPER[3], Y. GRIBOV[3], and J. SNIPES[3]

[1]Lehigh University, Bethlehem, PA, USA
[2]Princeton Plasma Physics Laboratory, Princeton, NJ, USA
[3]ITER Organization, CS 90 046, 13115 St. Paul Lez Durance, France

E-mail: kritz@lehigh.edu

Abstract. ITER hybrid and target steady state fusion burn scenarios are simulated using the PTRANSP integrated modeling code together with input from the TSC code. In the hybrid scenarios, the majority of the current is driven inductively; whereas, for the target steady state scenarios, approximately 22% of the current (at 1000 seconds) is driven inductively with the remaining current driven by the bootstrap, neutral beam and radio frequency sources. Predictive simulations are carried out using either the new Multi-Mode or GLF23 anomalous transport model. GLF23 simulations are carried out with different choices of moment transport: $\chi_\phi = \chi_{\phi,\mathrm{GLF23}}$ or $\chi_\phi = \chi_{i,\mathrm{GLF23}}$. The simulations of the hybrid scenario indicate that at 1000 sec the fusion power production will be 500 MW corresponding to a fusion Q = 10.0. The fusion power predicted in the simulations of the steady state scenarios is found to depend on the time history of the input heating and associated current drive. The fusion power obtained in the target steady state scenarios, depending on transport model and heating history, ranges from 88 MW up to 180 MW.

1. Introduction

Detailed scenario modeling of hybrid and target steady state ITER discharges is carried out as an aid in preparing for the commissioning of ITER and for the fusion burn stages of the ITER operation. The simulation results presented are obtained using the PTRANSP predictive integrated modeling code with time evolved boundary conditions and the plasma shape provided by the free boundary Tokamak Simulation Code (TSC) [1].

The simulations involve two types of discharge scenarios: (1) hybrid scenarios with I_p = 12.5 MA and $n_{e,20}(0)$ = 0.89 during the flat-top portion of the discharge; and (2) several target steady state scenarios with I_p up to 9 MA and $n_{e,20}(0)$ = 0.75 during the flat-top. The density as function of square root of poloidal flux is show in Fig. 1 for a hybrid discharge and the target steady state scenarios at 1000 seconds. Previously, ITER modeling was carried out for ELMy H-mode scenarios with I_p = 15 MA and $n_{e,20}(0)$ = 1.0 during the flat-top burn [2,3]. Fusion burn simulations are carried out using deuterium-tritium fuel together with a prescribed impurity concentration (2% He^3, 2% beryllium and argon in the range 0.12% to 0.5%) in the discharges considered) as well as the accumulation of helium ash from the fusion reactions. Scenarios are modeled to determine the characteristics of current drive, power deposition, and fusion power production.

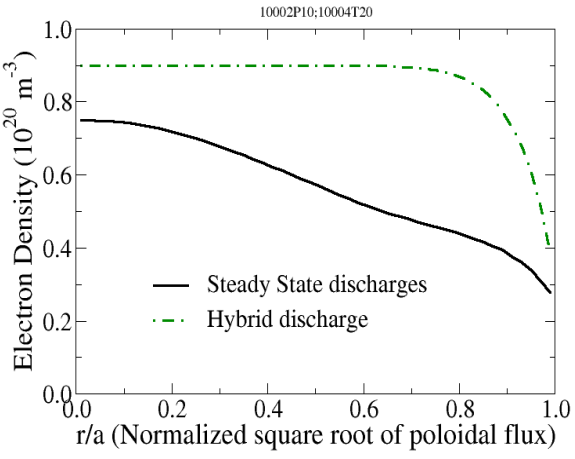

Fig. 1. Electron density profile for target steady state and hybrid discharges at t = 1000 seconds.

In the simulations, the evolution of the plasma discharge is followed from the early start-up stage, with plasma current as low as 0.5 MA and correspondingly low density, to full current and density during the burn stage. The ramp-up stage of the discharges studied is of the order of 150 seconds. Low levels of heating are used during the ramp-up stages in order to freeze in a broad current density profile. The intent is to avoid or delay sawtooth oscillations, by maintaining $q_{axis} > 1$, or to produce a reversed magnetic shear configuration for advanced tokamak scenarios. Feedback loops are used in TSC simulations to control the plasma position and shape while constraints are used for the maximum allowed coil currents. The time evolution of the plasma boundary position and shape, just inside the separatrix, is passed from the TSC code to the PTRANSP code, in which the prescribed-boundary version of the TEQ module [4] or VMEC [5] is used to compute the self-consistent evolution of the equilibrium.

PTRANSP simulations are carried out using either a new version of the Multi-Mode transport model [6] or the GLF23 anomalous transport model [7]. The momentum transport and flow-shear suppression features of the new Multi-mode transport model are utilized to compute the toroidal angular frequency profile and possible resulting internal transport barriers. The Multi-Mode and GLF23 anomalous transport models are quite "stiff" in the sense that local transport increases rapidly with increasing temperature gradient above a threshold. One consequence of stiff transport is that fusion power excursions rapidly damp out. Since fusion Q increases substantially with decreasing auxiliary heating power, fusion Q is maximized by decreasing the auxiliary heating power to levels just above the H-mode threshold.

The NCLASS module [8] is used to compute neoclassical ion thermal transport as well as neoclassical resistivity and bootstrap current for the evolution of the q profile. The procedures followed in setting up these ITER simulations are consistent with the procedures that have been used previously in carrying out simulations in which resulting profiles are compared with experimental data from existing tokamaks.

Auxiliary heating sources are computed in PTRANSP using the NUBEAM module [9] for neutral beam injection, the TORIC full wave module [10] for ICRF, the TORAY module [11] for electron cyclotron, and the LSC 1-D Fokker Planck module [12] for lower hybrid. Atomic physics cross sections for ionization, recombination and impurity radiation are computed using the ADAS [13] in the PTRANSP code. Fusion reaction rates are computed using the NTCC PREACT module (http://w3.pppl.gov/NTCC/PREACT). The baseline value of the H-mode pedestal height is computed using the EPED1 model [14].

2. Simulation Results

Contributions to the total plasma current in the hybrid discharge (12.5 MA) and in the target steady state discharge (9.0 MA) are shown in Figs. 2 and 3 as a function of time. These results are obtained in PTRANSP predictive simulations using the Multi-Mode transport model. It can be seen that the bootstrap current provides the largest contribution to the non-inductive current in both scenarios (4.0 MA for the hybrid discharge and 3.0 MA for the steady state discharge). The bootstrap current accounts for approximately one third of the total current driven in the steady state scenario. Nearly two thirds of the current is inductively driven in the hybrid scenario while less than one-quarter of the total current is inductively driven in the later stages of the target steady state scenario. The current, other than bootstrap current, is driven by neutral beam and lower hybrid heating. In the simulations, the ion cyclotron driven current is not included but is expected to be of the order

0.5 MA from previous TORIC calculations. (The omission of the ion cyclotron current drive provides a small margin with regard to the current that must be driven other sources). In Figs. 2 and 3, it is shown that the discharges are simulated from the low current start up stage well into the flat-top burn phase of the discharge. Typically predictive PTRANSP simulations are carried out for discharge times of the order of 1000 seconds, but the current drive results do not change appreciably with time when the input power remains unchanged. The amount of bootstrap current differs by a few tenths of a MA depending upon the transport model and the conditions of the simulation.

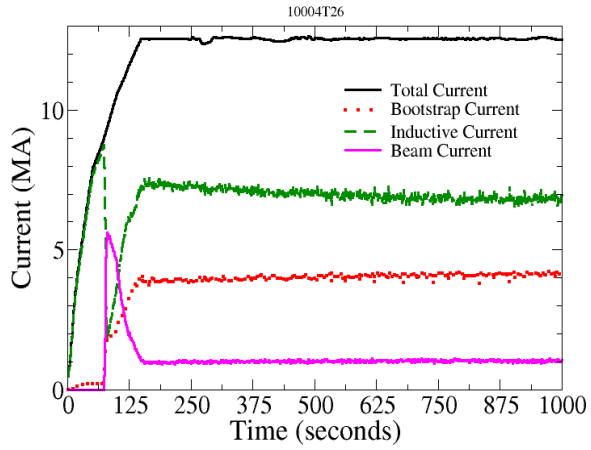

Fig. 2. Components of current as a function of time for a hybrid ITER discharge simulation.

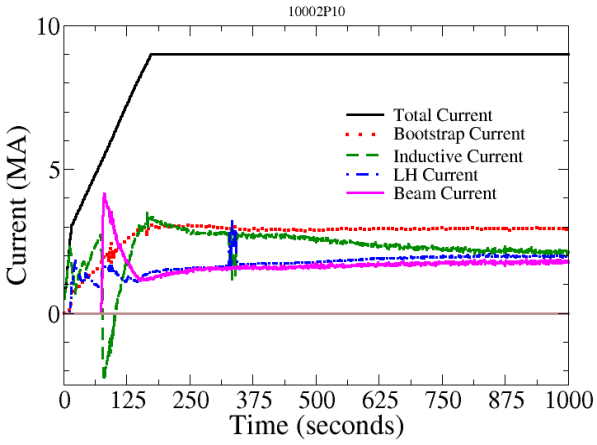

Fig. 3. Components of current as a function of time for a target steady state ITER discharge simulation.

Different components of current density (Ohmic, bootstrap, NBI and RF) are driven in different parts of the plasma. It can be seen in Figs. 4 and 5 that the bootstrap current density is driven across most of the plasma radius while the Ohmic and NBI current are driven primarily near the center of the plasma. Lower hybrid current, for the case shown in Fig. 5, is driven in the outer half of the plasma. There is a spike in the bootstrap current in the pedestal region at the edge of the plasma.

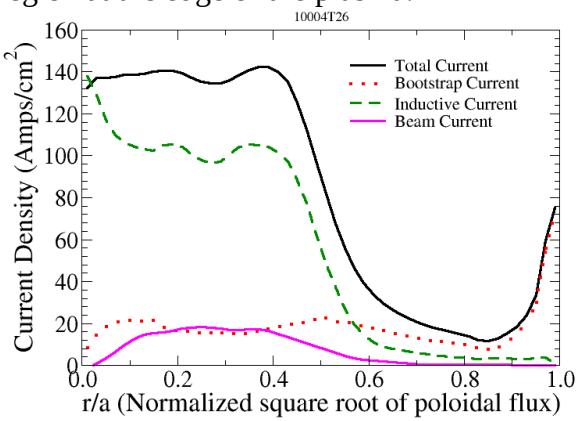

Fig. 4. Components of current density as a function of normalized minor radius at t=1000s for a hybrid ITER discharge.

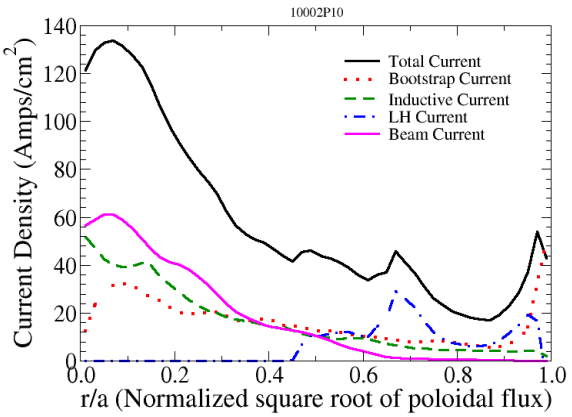

Fig. 5. Components of current density as a function of normalized minor radius at t=1000s for the target steady state discharge.

The *q*-value in the central region of the plasma remains close to unity at all times during both the hybrid and target steady state discharge simulations. In simulations in which *q* drops below unity, the Porcelli model is used to trigger sawtooth crashes. The *q* profile evolves over time scales of hundreds of seconds during each simulation. An illustration of the evolution of the *q* profile is shown in Fig. 6 representing three time slices in a selection of

three target steady state and one hybrid simulation. The different steady state simulations differ in the form of the density and impurity concentration profiles. For example, in the ss02 case the argon impurity is 0.2%, in the ss04 case the argon impurity is 0.5%, and in the ss06 case the argon impurity is 0.4%. The evolution of the *q* profile and the toroidal angular rotation profile are found to have a significant effect on the transport and predicted fusion performance in these simulations, which will be described in more detail below.

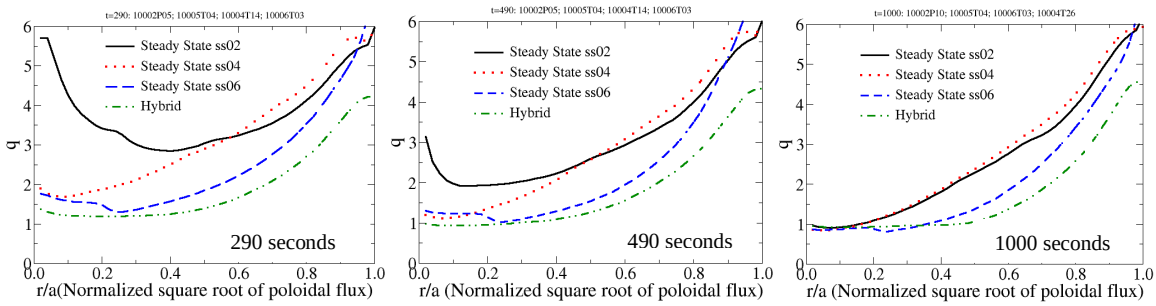

Fig. 6. q profile as a function of normalized minor radius for ITER simulations at 290 seconds, 490 seconds and 1000 seconds.

The current density and resulting *q* profiles can be modified by controlling the steering of the neutral beam injectors — by steering either on or away from the magnetic axis. In the ITER simulations, two 1 MeV neutral beams are used, each with 16.5 MW of power. Fig. 7 shows the effect on current density of steering one or both neutral beams on axis or off axis. It can be seen that NBI-driven current can be used to control the central current density, which is inversely proportional to the *q*-value. The total current with each flux surface, shown in Fig. 8, is less strongly affected by NBI steering. In fact, the total NBI current driven with the plasma (edge value in Fig. 8) is not affected at all by NBI steering. The NBI power deposition profiles are strongly affected by NBI steering, as can be seen from Fig. 9 below.

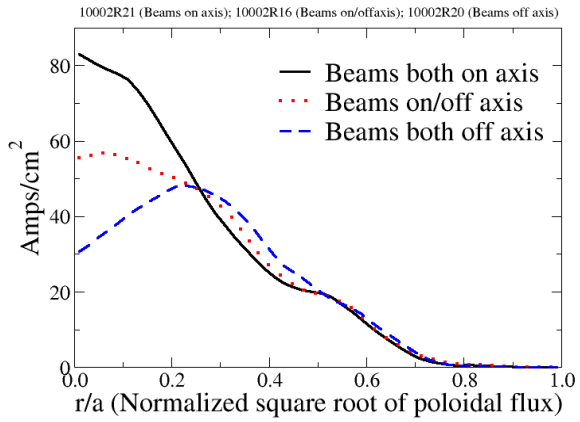

Fig. 7. Current density driven by neutral beams as a function of normalized minor radius for steady state ITER simulations illustrating the effect of NBI steering.

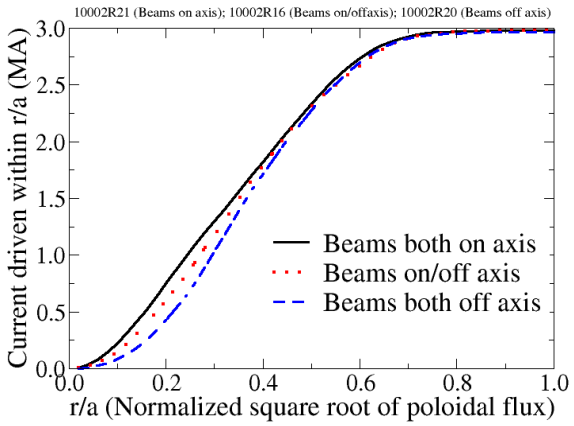

Fig. 8. Effect of NBI steering on total current driven by neutral beams as a function of normalized minor radius for steady state ITER simulations.

The ion cyclotron power deposition profiles can be controlled by changing the ion cyclotron frequency while holding the ITER magnetic field constant. In the simulations carried out, the ion cyclotron frequency was varied between 48.0 and 53.5 MHz, and the results shown below are for the low and high frequencies employed. With ion cyclotron heating there is a clear difference between the ion and electron power deposition profiles. These profiles are shown in the left and right panels, respectively, in Fig. 10. For the simulations shown in Figs. 10, a relative concentration of 2% He^3 provides for the absorption by minority ions. Ion damping

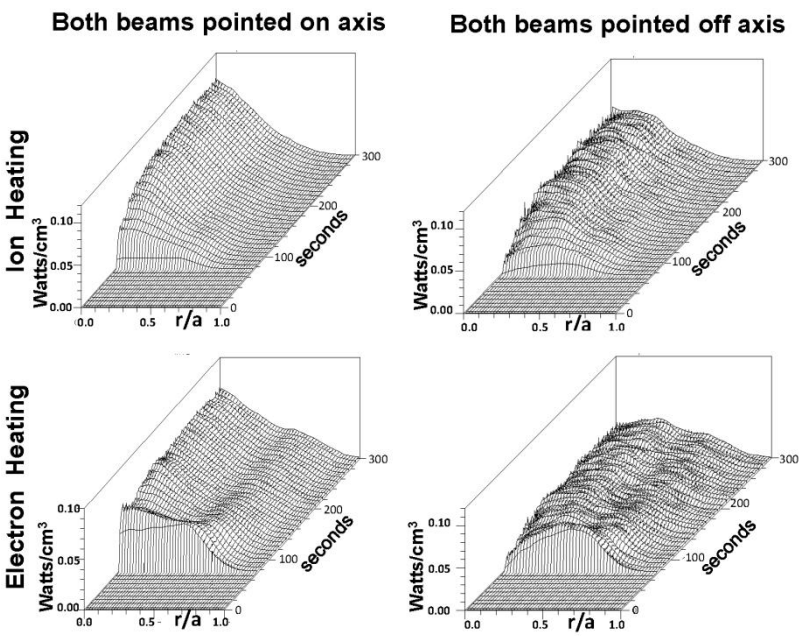

Fig. 9. Effect of NBI steering on the ion and electron power deposition profile as a function of normalized minor radius and time for steady state ITER simulations.

occurs on the high magnetic field side of the magnetic axis, with the damping occurring at smaller values of major radius for 53.5 MHz frequency than for the case in which the ion cyclotron frequency is 48.0 MHz. In the simulation with 48.0 MHz there is some on-axis ion damping, as shown in the left panel in Fig. 10. The shape of the electron power deposition profiles (right panel) are noticeably different from the ion power deposition profiles (left panel) because electrons absorb power from Landau damping close to the magnetic axis as well as absorbing power from the slowing down of fast minority ions. At lower frequencies, more ion cyclotron power is deposited to the ions than to the electrons and the power is deposited closer to the magnetic axis. Note that as a consequence of the Shafranov shift, there is a strong outward shift in the magnetic axis to a major radius of seven meters.

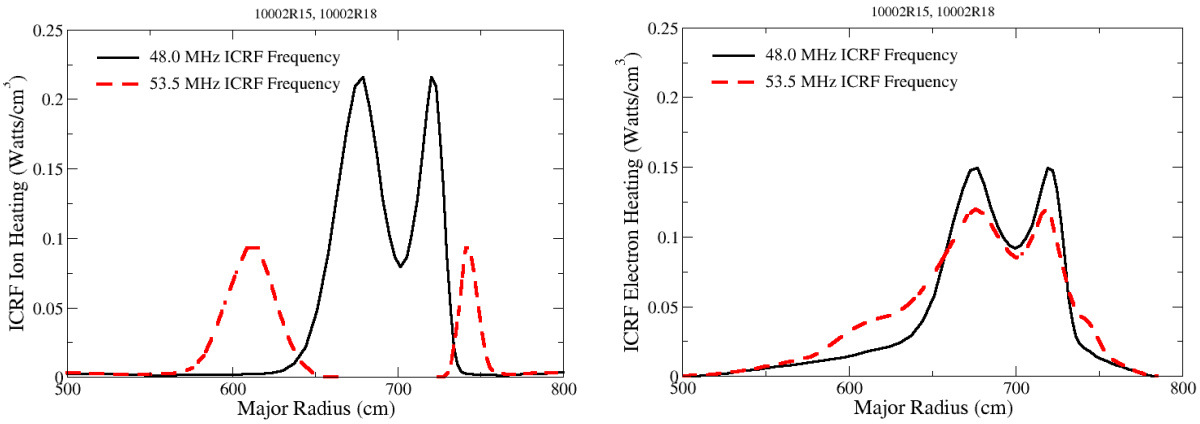

Fig. 10. Effect of changing the ICRF frequency on the ion and electron power depositon profile as a function of major radius in ITER steady state simulations.

Predictive simulation results depend on the anomalous transport model that is being used, as shown in Fig. 11. In these simulations of an ITER hybrid discharge, the electron and ion pedestal temperature is taken to be 5 keV, consistent with EPED1 predictions. The ICRF frequency is set to 48.0 MHz and both beams are pointed off axis. The Multi-mode model includes a momentum pinch effect that pulls toroidal angular momentum in from the edge of the plasma where the angular frequency was set to 30 krad/s, consistent with corresponding DIII-D simulations. When the GLF23 model is used, there are two choices of models used for momentum transport: The dashed red curve in Fig. 11 shows results when using momentum transport computed by the GLF23 model while the chained blue curve shows results obtained with the momentum diffusivity set equal to the ion thermal diffusivity

computed by the GLF23 model. It can be seen in Fig. 11 that at 1000 seconds the higher angular toroidal frequency obtained when using the Multi-Mode model results in much higher ion temperature profile in the core region. However, as shown in Fig. 12 below, although the simulation using the Multi-Mode model predicts higher fusion power at early times, the fusion power predicted in simulations using GLF23 and Multi-Mode are comparable at 1000 seconds. Both Multi-mode and GLF23 simulations employ the same density profiles.

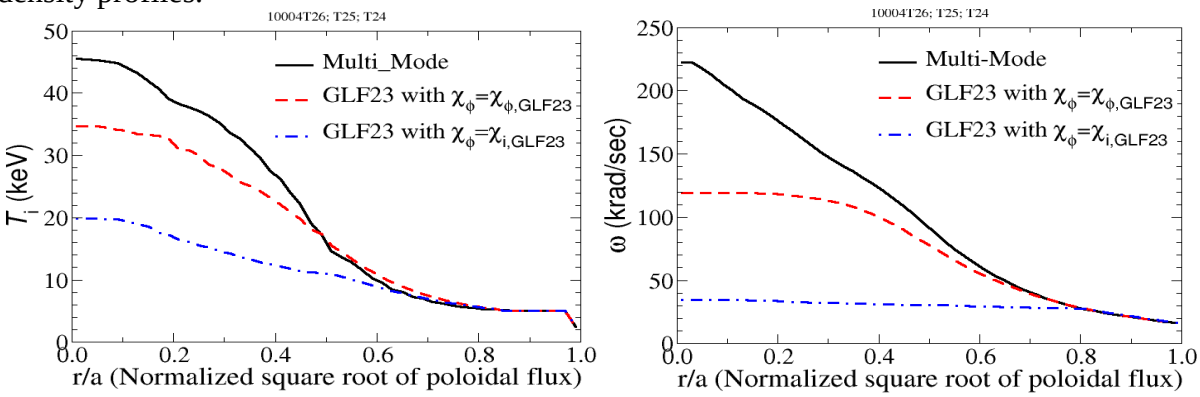

Fig.11. Ion temperature (left panel) and toroidal angular frequency (right panel) as a function of normalized minor radius for simulations using Multi-Mode (solid curves) and GLF23 (dashed curves) anomalous transport models at 1000 seconds during hybrid ITER simulations.

3. Fusion power production predictions

The fusion power production is shown as a function of time in Fig. 12 for hybrid scenario simulations using the Multi-Mode and GLF23 transport models. The conditions for these simulations are the same as those described in Fig. 11. It can be seen in Fig. 12 that the fusion power production in the Multi-Mode simulation initially grows very rapidly with time and then slows down relative to the growth of fusion power with time in the GLF23 with $\chi_\phi = \chi_{\phi,GLF23}$ simulation. At 1000 seconds the fusion Q (= fusion power / auxiliary power) is 10.0 for the Multi-Mode simulation and 6.0 and 9.9 for the two GLF23 simulations The fusion power production increases during the 1000 second simulation because the q profile and the toroidal angular rotation continue to evolve during that time.

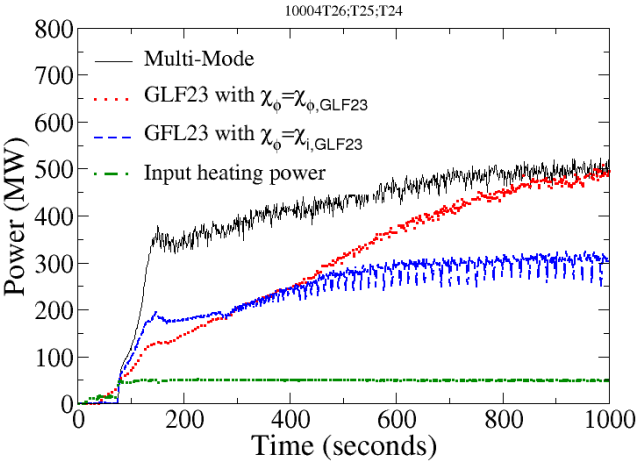

Fig. 12. Fusion power production is shown as a function of time for ITER hybrid simulations using the Multi-Mode and GLF23 transport models. Auxiliary input heating power is shown in the bottom curve.

The fusion power is considerably less in the target steady state scenarios, as illustrated in Fig. 13 for a Multi-Mode simulation with 79 MW of auxiliary heating power. The peak fusion power production in this simulation is 136 MW for a fusion Q equal to 1.72. Surprisingly, if the ICRF and Lower-Hybrid auxiliary power are turned off at 500 seconds, the fusion power production continues to increase to higher values as illustrated in Fig. 14 for steady state ITER simulations using the Multi-Mode and GLF23 ($\chi_\phi = \chi_{\phi,GLF23}$) transport models.

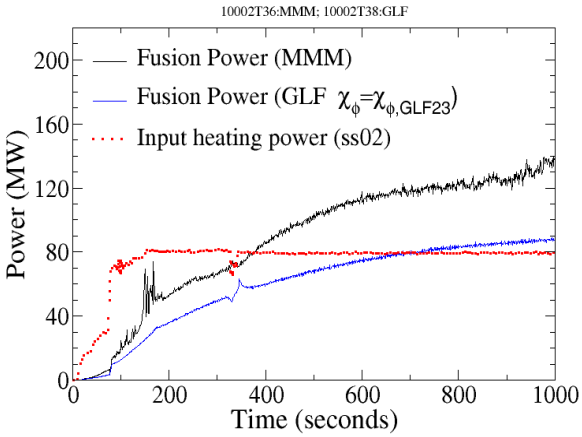

Fig. 13. Fusion power production and auxiliary heating power are shown as a function of time for a target steady state SS02 simulation using the GLF23 and Multi-Mode transport models.

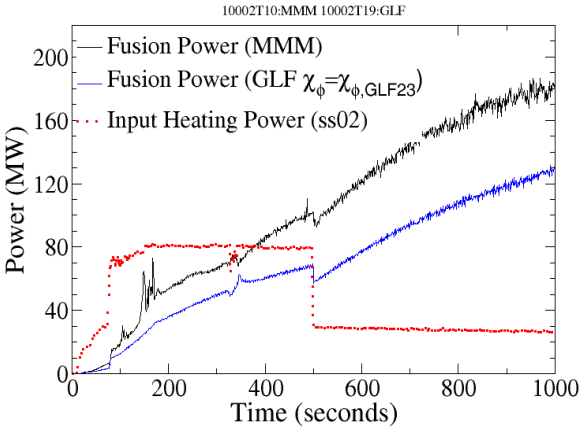

Fig. 14. Fusion power production is shown as a function of time for ITER simulations, similar to those in Fig. 13, but in which the RF power is turned off at 500 seconds.

The fusion power continues to increase because the *q* profile continues to evolve, as shown in Fig. 15a, in response to the more centrally peaked current driven by NBI. (Note, as shown in Fig. 5, the lower hybrid power which is turned off at 500 seconds drives current in the edge region of the plasma.) The increasingly peaked current density results in lower values of central q, decreasing the connection length, which increases the stabilizing field-line bending

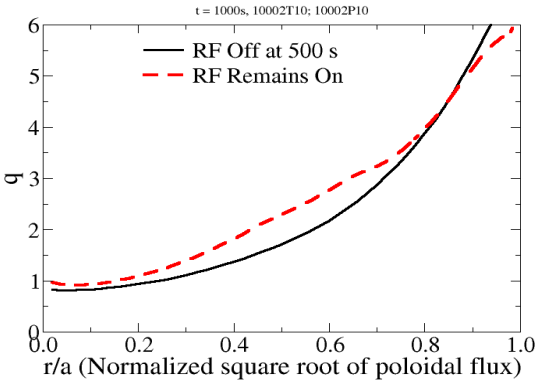

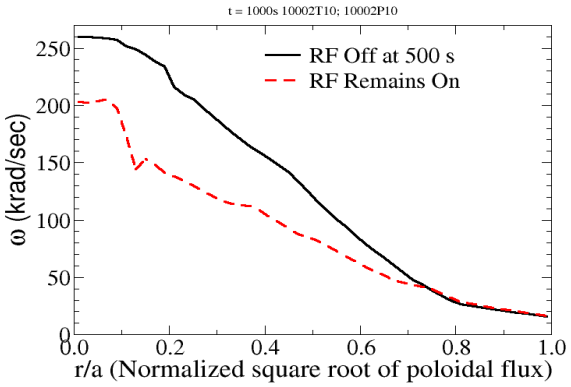

Fig. 15. (a)(Left panel) q profile and (b) (Right panel) Toroidal angular frequency as a function of normalized minor radius for target steady state ITER simulations at t=1000 seconds. The solid curve indicates the simulation result with input power remaining constant during the entire simulation and the dashed curve, with the RF power is turned off at 500 seconds.

as well as sound wave effects that result in a reduction of the drift-wave transport. The resulting decrease in the drift-mode transport causes the toroidal angular frequency profile to increase in the plasma core, as illustrated in Fig. 15b. The combined effect of the *q* profile and the increased flow shear resulting from the torodial angular frequency profile reduces the thermal transport as shown in Fig. 16a and results in an increase in the ion temperature profile, as illustrated in Fig. 16b. The pedestal temperature in these steady state simulations is taken to be 3.7 keV, consistent with EPED1 predictions. By the end of the Multi-Mode simulation, the fusion power is 180 MW and the fusion *Q* is 6.66. By the end of the corresponding GLF23 simulation, the fusion power is 130 MW and the fusion *Q* is 4.81.

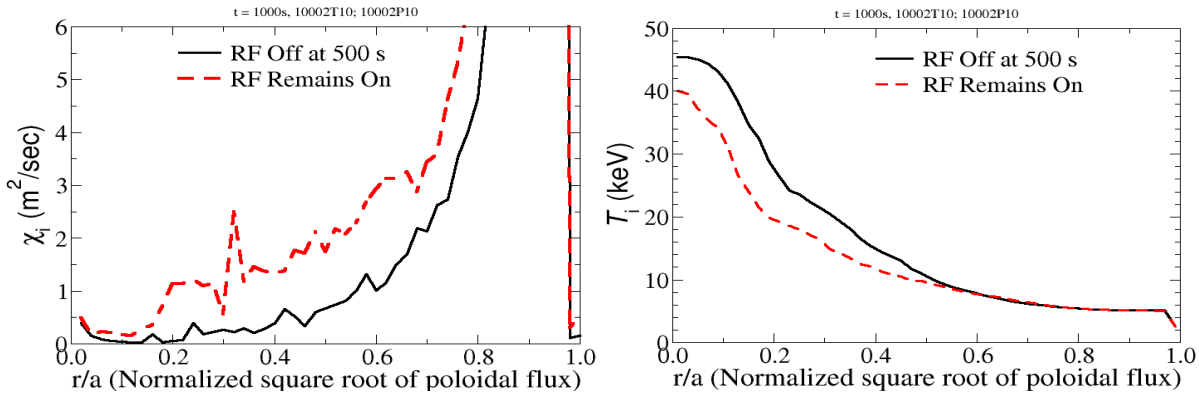

FIG. 16. (a) (Left panel) Ion conductivity and (b) (Right panel) ion temperature as a function of normalized minor radius for target steady state ITER simulations at t=1000 seconds. The solid curve indicates the simulation result with input power remaining constant during the entire simulation and the dashed curve, with the RF power is turned off at 500 seconds.

The fusion power and fusion *Q* predicted in the ITER simulations carried out are summarized in the table below:

Discharge	Transport model	RF Power off at 500s	Input power at 1000s MW	Fusion Power MW	*Q*
Hybrid	GLF23 with $\chi_\phi = \chi_{i,GLF}$	No	50	300	6.00
Hybrid	GLF23 with $\chi_\phi = \chi_{\phi,GLF}$	No	50	494	9.88
Hybrid	Multi-Mode	No	50	500	10.00
Steady State	GLF23 with $\chi_\phi = \chi_{\phi,GLF}$	No	79	88	1.11
Steady State	Multi-Mode	No	79	136	1.72
Steady State	GLF23 with $\chi_\phi = \chi_{\phi,GLF}$	Yes	27	130	4.81
Steady State	Multi-Mode	Yes	27	180	6.66

The views and opinions expressed herein do not necessarily reflect those of the ITER Organization.

[1] C. E. Kessel *et al.*, this conference; S. C. Jardin, et al., J. Comput. Phys., **66**, 481 (1986).
[2] F. D. Halpern *et al.*, Phys. Plasmas **15**, 065033 (2008).
[3] R. V. Budny, Nucl. Fusion **49**, 085008 (2009).
[4] L. L. LoDestro and L. D. Pearlstein, Phys. Plasmas **1**, 90 (1994).
[5] S. P. Hirshman *et al.*, Comput. Phys. Commun., **43**, 143 (1986).
[6] F. D. Halpern *et al.*, Phys. Plasmas **15**, 012304 (2008); J. Weiland *et al.*, Nucl. Fusion **49**, 965933 (2009); G. Bateman *et al.*, Plasma Phys. Control. Fusion **48**, A93 (2006); W. Horton, *et al.*,Phys. Plasmas **7**, 1494 (2000); T. Rafiq *et al.*, Phys. Plasmas **17**, 082511 (2010); J. D. Callen, Phys. Plasmas **12**, 092512 (2005).
[7] R. E. Waltz *et al.*, Phys. Plasmas **4**, 2482 (1997); G. M. Stabler *et al.*, Nucl. Fusion **37**, 287 (1997); J. E. Kinsey *et al*, Phys. Plasmas **12**, 052503-1 (2005).
[8] W. A. Houlberg *et al.*, Phys. Plasmas **4**, 3230 (1997).
[9] A. Y. Pankin *et al.*, Comp. Phys. Commun. **159**, 157 (2004); R. J. Goldston *et al.*, J. Comput. Phys. **43**, (1981).
[10] M. Brambilla, Max-Planck-Inst. report IPP 5/66 (1996).
[11] A. H. Kritz *et al.*, Proc. 3rd Joint Varenna-Grenoble Int. Symp. Grenoble **2,** 707 (1982).
[12] D. W. Ignat *et al.*, Nucl. Fusion **34**, 837 (1994).
[13] H. P. Summers *et al.*, AIP Conf. Proc. **901**, 239 (2007); http://open.adas.ac.uk.
[14] P. B. Snyder *et al.*, Phys. Plasmas **16**, 056118 (2009).